Front. Environ. Sci. Eng. 2020, 14(4): 70
https://doi.org/10.1007/s11783-020-1249-6

RESEARCH ARTICLE

Synthesis of vinasse-dolomite nanocomposite biochar via a novel developed functionalization method to recover phosphate as a potential fertilizer substitute

Nima Kamali[1], Abdollah Rashidi Mehrabadi (✉)[1], Maryam Mirabi[1], Mohammad Ali Zahed[2]

1 Civil, Water and Environmental Engineering Faculty, Shahid Beheshti University A.C., Tehran, Iran
2 Cell and Molecular Biology Department, Faculty of Biological Sciences, Kharazmi University, Tehran, Iran

HIGHLIGHTS

- Nanocomposites were prepared by adding dolomite to vinasse at different ratio.
- Textural and morphological features of adsorbents were studied in detail.
- CCD based RSM was used for investigation of P ion removal by nanocomposite.
- The q_m based on Langmuir model for modified vinasse biochar was 178.57 mg/g.
- P loaded nanocomposite improved plant growth and could be utilized as P-fertilizer.

GRAPHIC ABSTRACT

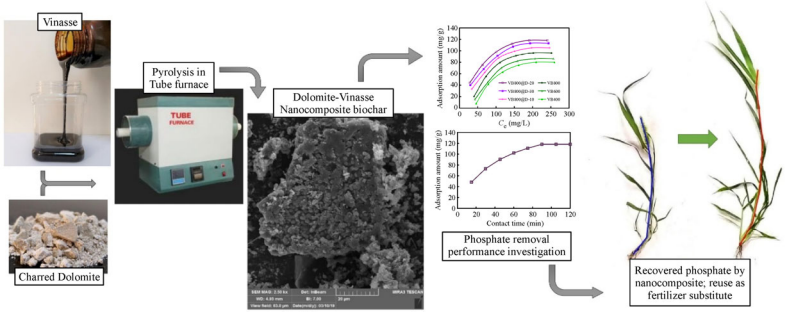

ARTICLE INFO

Article history:
Received 4 December 2019
Revised 17 February 2020
Accepted 21 March 2020
Available online 30 April 2020

Keywords:
Biochar
Vinasse
Dolomite
Phosphate
Fertilizer

ABSTRACT

The effectiveness of phosphate (P) removal from aqueous solutions was investigated by novel low-cost biochars synthesized from vinasse and functionalized with calcined dolomite. The vinasse-derived biochar, synthesized via pyrolysis at different temperatures, showed easy preparation and a large surface area. The novel vinasse biochar nanocomposites were prepared by adding dolomite to the vinasse biochars with different weight percentages (10, 20 and 30%). The characteristics of the prepared materials were identified for further understanding of the inherent adsorption mechanism between P ions and vinasse biochars. Vinasse-dolomite nanocomposite was very effective in the adsorption of P species from aqueous media. The effect of the operational factors on Vinasse-dolomite nanocomposite was explored by applying response surface methodology (RSM). According to RSM results, the optimum condition was achieved to be contact time 90 (min), 250 (mg/L) of P concentration and pH 7. Thermodynamic isotherm and kinetic studies were applied on experimental data to understand the adsorption behavior. The Vinasse-dolomite nanocomposite revealed preferential P species adsorption in the presence of co-existing anions. The P species could be recovered by 1.0 M HCl where the efficiency was not affected up to the fifth cycle. The P-loaded Vinasse-dolomite nanocomposite was successfully tested on a plant; it significantly improved its growth and proved its potency as a P-based fertilizer substitute.

1 Introduction

Phosphate (P) is recognized as being one of the critical global resources that will be depleted by the end of this century (Pradel and Aissani, 2019). More than 90% of phosphates are applied in phosphatic fertilizers, approximately 7% in detergents, and the rest in other applications (Huang et al., 2017b). Excess discharge of P from agricultural and industrial productions to aqueous media causes eutrophication (Sun et al., 2018) leading to dissolved oxygen depletion and fish toxicity, growth of blue and green algae, deterioration of water quality, and hence impaired public health (Boeykens et al., 2017). Thus, it is urgent to develop promising P removal methods from water synchronously.

Multiple studies have been conducted to maintain a low

✉ Corresponding author
E-mail: a_rashidi@sbu.ac.ir

level of redundant P in water or wastewater, including membrane filtration, ion exchange, biological treatment, chemical precipitation, and adsorption (Huang et al., 2017a; Ren et al., 2017). Biological treatment is extremely vulnerable to fluctuations in characteristics of wastewater, leading to low reliability and stability (Ye et al., 2016). Precipitation through chemical process costs require purchasing chemicals and transportation, and leads to undesired waste sludge which ought to be effectively managed (Li et al., 2018b). Membrane filtration is limited by fouling and is economically unattractive (Shahid et al., 2019), while ion exchange may lose its adsorption capability after multiple regenerations. On the other hand, adsorption is thoroughly recommended as a feasible process for treating P (Selim et al., 2019). The main challenge for the adsorption method is to find inexpensive materials which simultaneously have a fast adsorption rate and high adsorption capacity. Various adsorbents such as industrial by-products and agricultural wastes have been successfully tested in the adsorptive removal of P (López et al., 2019).

Over the last decades, several authors have focused on biochar as an adsorbent for removing contaminations from water streams, which could exert useful effects for both carbon sequestration and water pollution control (Wang and Wang, 2019). Furthermore, there is no need to recycle the spent biochar since after P adsorption, it can be directly applied to the soil, bringing fertility and building soil carbon (Vikrant et al., 2018). Indeed, based on previous studies, in the presence of MgO and CaO, the P adsorbed on to the biochars, has proven benefits on plant growth (Yao et al., 2013; Li et al., 2016b; Li et al., 2018a). Biochar is a generally stable black carbon byproduct materials derived from pyrolyzing biomass under little or no oxygen conditions (Xue et al., 2019). The utilization of locally available and low-cost biomass for biochar fabrication is an emerging interest in the scientific community. The potential use of biochar obtained from indigenous and renewable biomass is commonly considered to be a proper economic and environmental policy for waste recycling and P treatment (Valle et al., 2016). Biochar can be made of numerous waste biomass sources (Tripathi et al., 2016).

Vinasses are a liquid waste extracted during ethanol production from sugar beet or sugarcane as well as distillation of beverages (Fukushima et al., 2019). On average, every liter of produced ethanol generates approximately 10–15 L of vinasse. The chemical composition of waste vinasse changes based on the raw material applied for ethanol production and the distillation process (Hoarau et al., 2018). They are characterized by a dark brown color, high electrical conductivity, low pH (pH 3.5–5.0), high concentrations of suspended and volatile solids, large amounts of organic substances (COD: 50–150 g/L), and occasionally contain heavy metals such as magnesium (Mg), calcium (Ca), potassium (K), etc (Aparicio et al., 2017). Biochar derived from vinasses has a large surface area, porous structure, and abundant functional groups, and thus may be effective for the removal of P from aqueous solutions (Kazak et al., 2017). Vinasse can be treated by biological and physicochemical processes, which can reduce its toxicity through degrading its organic components. Thus, it can totally or partially replace the use of chemical fertilizers, especially those containing P, thereby reducing crop costs. Discharging vinasse to water bodies or soil without any treatment would cause numerous environmental issues such as disorganization in fish tissue, death of aquatic organisms, and contamination of portable water sources (Chowdhary et al., 2017; Hoarau et al., 2018) as well as soil toxicity and quality changes (Christofoletti et al., 2013).

Some of the typical methods of adsorbent modification are ion exchange, wet and dry impregnation and physical mixing procedures. This study suggests a new strategy to enhance the adsorption efficiency of the original vinasse-derived biochar (VB) by adding mineral oxides. Intermixing mineral oxides with VB leads to appearance of unique chemical and physical properties associated with improved the rapidity of adsorption.

Dolomite, a popular mineral rock and available in sedimentary thick beds, can also be found in hydrothermal veins, metamorphic marbles, and replacement deposits (Zhao et al., 2018). It has gained a great deal of attention for more than six decades due to its inexpensiveness and universal availability. The overall formula of dolomite is usually $MgCa(CO_3)_2$. The amount of magnesium and calcium in most specimens is identical, but sometimes one element might have a slightly higher presence than the other. Small amounts of manganese and iron are also occasionally present (Nugroho et al., 2014).

The goals of this study were to develop a VB-dolomite nanocomposite for the removal of P species from aqueous media and evaluate its performance as P substitutive fertilizer. Thus, vinasse of sugar beet was obtained locally and pyrolyzed at different temperatures. The morphological and textural features of prepared carbonous materials were investigated by various techniques. RSM based on central composite design (CCD) was applied for the experimental design in order to minimize the number and duration of experiments and optimize the removal conditions of P ions by VB800@D-20. The adsorption properties of the as-synthesized nanocomposite such as thermodynamics, isotherms, and kinetics were studied. Desorption study was conducted on the prepared adsorbent to survey its potency to be regenerated based on the strength of the P-adsorbent bond. The efficiency and adsorption mechanism for P removal by the modified biochar and its performance as P-based fertilizer substitute were also examined.

2 Experimental

2.1 Preparation of VB

Condensed vinasse was obtained from an ethanol industry located in the north-west of Iran. A boiler was used to reduce the volume of vinasse to one-third, resulting in condensed vinasse.

Before the synthesis of VB, condensed vinasse was fully dried in oven for 12 h at 100°C. The dried vinasse was pyrolyzed in a pyrolysis reactor within three temperature ranges from ambient until the desired point (400°C, 600°C and 800°C) with the pace of 10°C/min under the N_2 flow of 100 mL/min and kept at the peak temperature for 60 min before cooling to the ambient temperature.

Finally, the obtained carbonous material was crushed and washed with deionized water five times to wipe the residual surface ash, and finally oven-dried at 100°C for 12 h before using in any experiment. The pyrolyzed dried vinasse at three temperatures (400°C, 600°C and 800°C), were labeled VB400, VB600 and VB800, respectively and applied for the study of P recovery from aqueous solutions and release.

2.2 Preparation of VB-dolomite nanocomposite

VB-dolomite nanocomposite was prepared according to the pyrolysis process of vinasse with dolomite as follows: Initially, raw dolomite was calcined in a furnace at 1200°C to become more active and porous (Salameh et al., 2015). Secondly, the calcined dolomite was stirred with raw vinasse (without any dehydration) at different weight ratios (10, 20 and 30%). Then, the composite, was pyrolyzed at 800°C in a furnace under 100 mL/min purging of N_2 gas. The obtained samples were named as VB800@D-10, VB800@D-20 and VB800@D-30, respectively.

2.3 Characterization

X-ray Fluorescence Spectroscopy (XRF) analysis was utilized for further and more accurate identification of samples and elemental composition (PW1410, Philips). For the unmodified and modified carbonous materials, Fourier transform infrared spectroscopy (FT-IR) spectra were obtained. The morphological features and chemical composition of VB adsorbents were further analyzed by scanning electron microscopy (SEM, MIRA III energy dispersive X-ray spectroscopy equipped electron microscope (EDX)). The crystallinity of the as-prepared adsorbents was investigated by X-ray diffraction (XRD) via Philips PW1730 diffractometer with Cu Kα radiation, at 40 kV and 20 mA. The textural properties of the VB prepared biochars were determined by N_2 adsorption/desorption via Micromeritics model ASAP 2010 sorptometer. To monitor the pH level of the solution in experiments, Fisher Scientific Accumet Basic AB15 pH meter was used. Pyrolysis process was carried out in a horizontal tube furnace (TF5/40-1500 AZAR FURNACES), with the maximum degree of 1500°C.

2.4 Phosphate adsorption experiments

For adsorption experiments, solutions of potassium phosphate monobasic (KH_2PO_4) were prepared in deionized water. The initial solution pH varied from 3.00 to 11.00 which was adjusted using 1 M NaOH or HCl solution. Adsorption isotherm studies were conducted in thermostatic shakers separately at 200 r/min and in 298 K. The initial (50, 150, 200, 250 and 300 mg/L) and equilibrium concentrations of P in experiments were measured by UV spectrophotometer. The percentage of P ion removal was calculated by Eq. (1):

$$R = \frac{C_0 - C_e}{C_0} \times 100\% \tag{1}$$

Meanwhile, the adsorption capacity of the adsorbent (q_e, mg/g) can be determined by Eq. (2):

$$q_e = \frac{(C_0 - C_e)V}{W}, \tag{2}$$

where C_e and C_0 represent the equilibrium and initial P ion concentrations in the solution, respectively (mg/L), W is the mass of dry adsorbent (g) and V denotes the solution volume (L).

2.5 Models for equilibrium and kinetic studies

The equilibrium adsorption capacity (q_e) and equilibrium concentration (C_e) were subjected to different isothermal models, including the Langmuir, Freundlich and D–R model.

The Langmuir isotherm could be expressed according to Eq. (3) (Langmuir, 1918):

$$\frac{C_e}{q_e} = \frac{1}{K_L q_m} + \frac{1}{q_m} C_e, \tag{3}$$

where q_m is Langmuir maximum adsorption capacity, which represents monolayer coverage of VB by the P ions, and K_L is also Langmuir constant related to the affinity of binding sites (L/mg).

The R_L, separation factor, is a dimensionless constant which can be used to express essential characteristics of the Langmuir isotherm according to Eq. (4):

$$R_L = \frac{1}{1 + R_L C_0} \tag{4}$$

The Freundlich isotherm model can be calculated according to Eq. (5) (Freundlich, 1907):

$$\ln q_e = \ln K_F + \frac{1}{n}\ln C_e, \quad (5)$$

where K_F is a constant describing the adsorption capacity (L/g) and n represents an empirical parameter related to the adsorption intensity.

The D–R isotherm model can be calculated according to Eqs. (6) and (7) (Dubinin and Radushkevich, 1947):

$$\ln q_e = \ln q_{DR} - K_{DR}\varepsilon^2, \quad (6)$$

$$\varepsilon = RT\ln\left(1 + \frac{1}{C_e}\right), \quad (7)$$

where KDR is D–R isotherm constant which describes the adsorption energy (mol2/Kj2), qDR represents the D–R adsorption capacity of an adsorbent (mg/g), ε is called Polanyi potential, T is the temperature (K), and R is the constant of ideal gas (8.314 J/mol K).

The magnitude of E, energy of P ion adsorption by prepared adsorbent, is a beneficial parameter to evaluate the type of the removal process and can be explained as Eq. (8) (Sivakumar and Palanisamy, 2009):

$$E = \frac{1}{(2K_{DR})^{0.5}}. \quad (8)$$

The P adsorption kinetic data were fitted into the pseudo-first-order, pseudo-second-order, Elovich, intraparticle diffusion and particle diffusion models. The linearized forms of these models are as follows, respectively:

$$\log(q_e - q_t) = \log q_e - \left(\frac{K_1}{2.303}\right)t, \quad (9)$$

$$\frac{t}{q_t} = \frac{1}{K_2 q_e^2} + \left(\frac{1}{q_e}\right)t, \quad (10)$$

$$q_t = \frac{1}{\beta}\ln(\alpha\beta) + \frac{1}{\beta}\ln t, \quad (11)$$

$$q_t = K_{int}t^{1/2} + C, \quad (12)$$

$$\ln\left(1 - \frac{q_t}{q_e}\right) = -K_p t, \quad (13)$$

where K_1 and K_2 are the rate constant for pseudo-first and-second order (L/min), (g/mg min), respectively; α and β represent the Elovich equation constants; K_{int} is the diffusion of the intraparticle coefficient (mg/g $min^{0.5}$) and K_p shows the particle rate constant (min^{-1}).

2.6 Thermodynamics studies

To evaluate the adsorption process in terms of being exothermic or endothermic and spontaneous or non-thermodynamic, variables such as changes in entropy, enthalpy and Gibbs free energy of the adsorption were determined from experimental data by the Equations below:

$$\Delta G = -RT\ln K_d, \quad (14)$$

$$\ln K_d = \frac{q_e}{C_e} \times C_s, \quad (15)$$

$$\ln K_d = \frac{\Delta S}{R} - \frac{\Delta H}{RT}, \quad (16)$$

where ΔG (kJ/mol), ΔS (kJ/mol/K) and ΔH (kJ/mol) are differences in the free energy, entropy, and enthalpy while K_d and C_s are equilibrium constant and solvent concentration, respectively.

2.7 Experimental design and central composite design (CCD)

RSM is definitely an effective strategy in designing, modeling, and optimizing conditions in a multivariable system (Karimifard and Alavi Moghaddam, 2018). In the present study, the five-level CCD, which is the most common form of RSM, was utilized for optimizing the adsorption process. Specifically, to analyze the effect of the operating parameters on the removal efficiency of P species, three influential factors were selected: contact time, initial pH, and initial P concentration. This system was designed Design Expert software version 10.0.7.0 in eight factorial points (2^n), six axial points ($2n$), and six central points (n_c), totally run in 20 obtained experiments by the following equation:

$$N = 2^{(n)} + 2n + n_c. \quad (17)$$

Based on the experimental range obtained, the levels of independent variables for P uptake are presented in Table S1 and S2 (in the supporting information file).

The results obtained from experiments were examined for the removal rate of P ions by VB800@D-20 nanocomposite, with each response correlated with the closest computed second-order polynomial model (Aksu and Gönen, 2006; Anbia and Rahimi, 2017):

$$Y = \beta_0 + \Sigma_{i=1}^{n}\beta_i X_i + \Sigma_{i=1}^{n}\beta_{ii}X_i^2 + \Sigma_{i=1}^{n}\Sigma_{j=1}^{n-1}\beta_{ij}X_i X_j, \quad (18)$$

where Y is the predicted response; β_i, β_0, β_{ii} and β_{ij} represent the linear coefficients, constant coefficient, quadratic coefficient and interaction coefficients, respectively.

2.8 Performance of biochar as P fertilizer

This study tried to develop a new adsorbent medium trapping dissolved P to recover it as a phosphorus fertilizer. To assess such performance and possibility, two evaluations were performed.

The first was a "release test" described in a previous study (Chen et al., 2014). Briefly, VB800@D-20 after P ion adsorption (VB800@D-20/P) was collected from the solution and dried in an oven at 100°C for 12 h. To analyze the release capability, VB800@D-20/P was added to 20 ml DI and shaken for 12 h at 3 pH levels 5, 6, and 7 with a magnetic stirrer. By filtering the biochar after the mentioned period, phosphate released to DI was determined. This capability, as reported by the mentioned study, is considered as the P-loaded biochar potential to use as a new source of P-fertilizer.

The second evaluation was done using VB800@D-20/P, as an alternative phosphate fertilizer in a pot experiment detailed in (Li et al., 2018a) which could be summarized as follows: planting 10 *Setaria viridis* (green foxtail) seeds in 2 pots with 800 g of the same soil type- collected from university greenhouse ground (at maximum depth of 25 cm), sieved for better uniformity and air-dried by expanding in flat area. In the first pot, 4.0 g of P-loaded biochar was mixed with the soil, while the second pot was kept as control to reflect the difference.

The pots were stored in a greenhouse with recorded temperature (19°C–22°C) and humidity (55%–65%). After 30 days, above soil surface heights and dry masses of *Setaria viridis* were measured and reported. To measure the dry weight, based on work of Creech et al., the harvested plants were kept in oven for 2 days at 60°C (Creech et al., 2004). The above procedure was done three times and the average values were reported.

3 Results and discussion

3.1 Prepared VB samples characterization

3.1.1 XRD analysis

The XRD spectra of VB samples and P adsorption on VB800@D-20 are shown in Fig. 1(a). The VB800@D nanocomposites showed peaks corresponding to VB800 and dolomite. Accordingly, the peak intensity of VB800@D was stronger than that of pure VB800. In the VB800@D spectrum, the peaks at $2\Theta = 18$ °, 34°, 37° and 54.07° were ascribed to CaO and the two strong peaks at $2\Theta = 43°$ and 62° were identified as MgO.

After P uptake on VB800@D-20, the intensity of the characteristic diffraction peak diminished, which can be ascribed to a reasonably strong binding of P ions to VB800@D-20, and more particularly, the metal oxides sites on VB800@D-20 (Chen et al., 2016).

3.1.2 FT-IR study

FT-IR spectra, identifying the functional groups in the compound, are shown in Fig. 1(b) for all prepared carbonous materials, both vinasse biochars and the modifies ones. The absorption peaks at 3400 cm^{-1}, 1600 cm^{-1}, 1410 cm^{-1}, 850–920 cm^{-1}, and 400–900 cm^{-1} of VB samples were constant and intensified upon pyrolysis temperature elevation. The presence of C = O, C = C, –COOH, CH_3O, and enhanced Mg–O and O–Mg–O were observed in VB samples. The absorption peaks at 3400 cm^{-1} increased with raising the pyrolysis temperature demonstrating the greater presence of C = O and C = C. As described in a previous study, during the pyrolysis over 400-450°C, poly-condensed aromatic carbon-type compounds could be shaped. The functional groups in the synthesized VB samples include methoxyl, carbonyl, carboxyl and hydroxyl which contributed to the adsorption.

FT-IR analysis performed on the VB800@D-20/P is also presented in Fig. 1(b). No significant differences were detected in the IR spectra, indicating similar functional groups as VB800@D-20 bands. The FTIR spectrum of P adsorbed VB800@D-20 showed new peak at 576 cm^{-1}. This is probably due to the bending vibration of O–P–O in

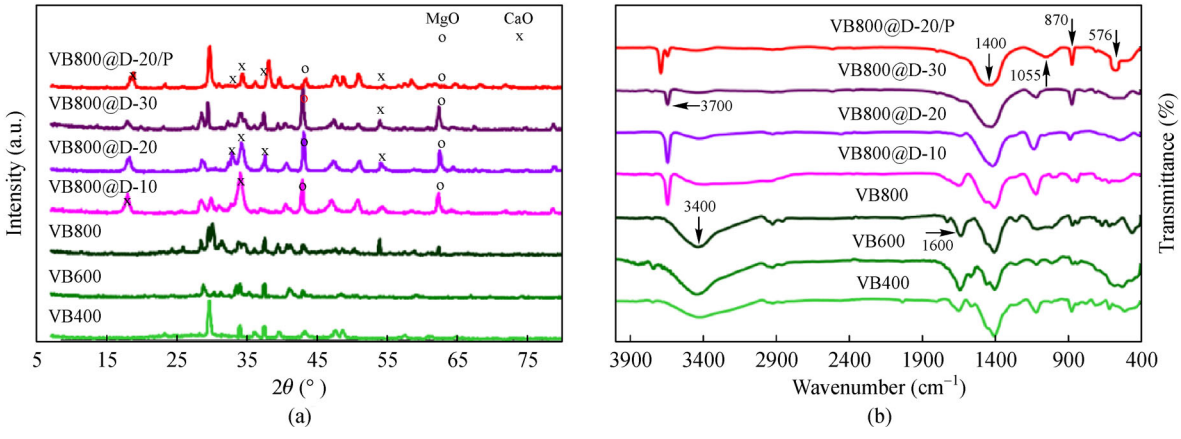

Fig. 1 (a) XRD patterns and (b) FT-IR spectra of the prepared VB samples.

PO_4^{3-} ionic groups. Further, a significantly increased band at 1055 cm^{-1} was related to the conventional features of the asymmetric stretch vibration of P–O.

3.1.3 SEM and EDX images

Fig. 2 displays the SEM-EDX micrograph of unmodified and modified VB samples. The surface morphology of VB samples indicated that the pyrolysis process was able to transform the liquid waste vinasse to the quasi-spherical carbonaceous materials. As shown in Fig. 2, the VB sample has a quasi-spherical shape with average diameters of approximately 10-50 nm. The surface of the VB samples appeared very similar as no major morphological differences could be seen.

According to the SEM image VB800@D nanocomposites, it was observed that the VB800@D possessed a compact and imperforate surface. As the dolomite content increased to 30 wt.%, the adsorbent particles agglomerated, indicating that a significant amount of dolomite fills in the space between the small carbon particles causing the pronounced agglomeration.

The EDX spectrum of the adsorbent surface also showed many elements detected in the elemental analysis. C, O, K, Mg and Ca were found in VB800@D nanocomposites as they are the major components of VB and dolomite. The SEM image of VB800@D-20 along with EDX spectra are also depicted in Fig. 2. Observations under SEM showed that the morphology and size of VB800@D-20 after loading the P ions remained almost intact.

The EDX analysis of VB800@D-20 after adsorption showed that P ions have been adsorbed successfully onto the VB800@D-20. This clearly confirmed the incorporation of P species into the VB800@D-20 matrix. The VB800@D-20/P had a remarkably high level of Mg, Ca and P. These results suggest that the VB800@D-20/P, when used in soils, may provide a more concentrated supply of nutrients to crops.

3.1.4 XRF analysis

The elemental composition of the as-synthesized materials is reported in Table 1. The main components of the prepared carbonous materials were organic matter in the form of organic acids and cations such as Ca, Mg and K. As presented in Table 1, the Ca and Mg contents in the VB samples considerably increased with the temperature rise of the pyrolysis. In order to check the dolomite effect on VB characteristics, the percentages of elemental compositions were also monitored. According to Table 1, an increase in the dolomite percentage from 10% to 30% induced a rise in the Ca and Mg contents. The presence of P in XRF analysis of VB800@D-20/P nanocomposite confirmed the adsorption of P ions.

3.1.5 N_2 adsorption-desorption isotherms analysis

Specific surface area is a remarkable factor which controls the performance of adsorption removal. The N_2 adsorption/desorption isotherms of VB samples at 77 K before and after modification were measured to evaluate their average pore size, total pore volume (V_{total}) and specific surface area (S_{BET}). Table 2 provides the textural characteristics of VB400, VB600, VB800, VB800@D-10, VB800@D-20, VB800@D-30 and VB800@D-20/P. The table indicates that the S_{BET} of VB-carbonous materials increased with synthesis temperature elevation. As the pyrolysis temperature rose (up to 800 °C), the removal of volatile organic compounds could occur more easily causing a significant increase in the porous structures of the as-prepared VB samples.

Based on Table 2, all the VB materials have an average pore diameter lower than 2 nm (< 2 nm), indicating the presence of micropores.

The results of VB800@D nanocomposites revealed that the compositing procedure has reduced the properties of VB800 texture. After the hybrid process, the dolomite was blocked in the pores and interlayers of VB800, inhibiting the N_2 molecules adsorption. As shown in Table 2, the porosity of dolomite modified carbons decreased when the mass ratio of dolomite to nanoporous carbons increased.

3.2 Seletion of suitable prepared adsorbents for the adsorption of P ions

The removal efficacy of biochar-based materials for different pollutions depends on its chemical and physical properties, which are significantly affected by the feedstocks, pyrolysis conditions (pyrolysis temperature, residual time, etc.) and technologies. Fig. 3 demonstrates the q_e trend versus equilibrium concentrations of P ions in the solution for unmodified and modified VB. The prepared adsorbents all revealed improved P adsorption with the rise of initial concentrations of P solutions and gradually reached saturation. The order of adsorption in terms of the amount adsorbed on the adsorbents is: VB800@D-20>VB800@D-30>VB800@D-10>VB800>VB600>VB400. The VB prepared at 400 °C showed a sorption capacity of 79 mg/g, a capacity which improved to about 85 mg/g for VB prepared at 600 °C and up to 96 mg/g for VB prepared at 800 °C. The observed enhanced performances from VB400 to VB800 can be ascribed to the changes occurring in the texture and surface area of VB samples during pyrolysis. With the heating temperature increase, the carbon content declined while the Mg and Ca contents increased in VB samples.

The results of adsorption experiments showed that phosphate adsorption mechanisms on metal oxides-modified biochars mainly include precipitation and electrostatic interactions with the infused metal oxides on

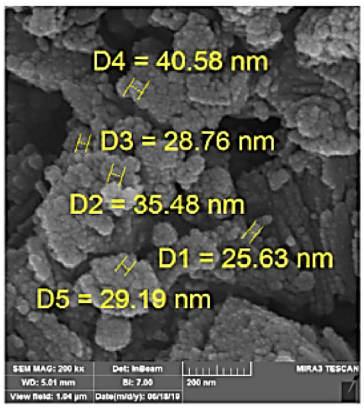
D4 = 40.58 nm
D3 = 28.76 nm
D2 = 35.48 nm
D1 = 25.63 nm
D5 = 29.19 nm

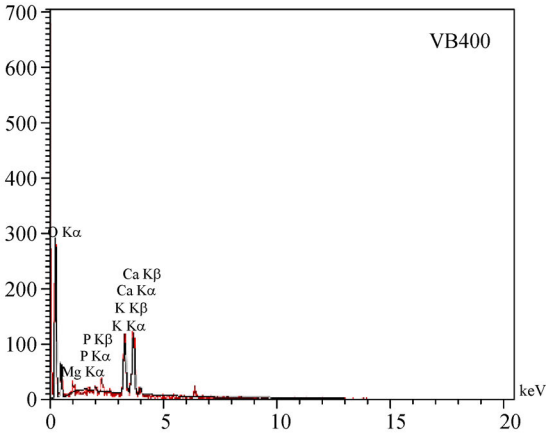
VB400
O Kα
Ca Kβ
Ca Kα
K Kβ
K Kα
P Kβ
P Kα
Mg Kα
keV

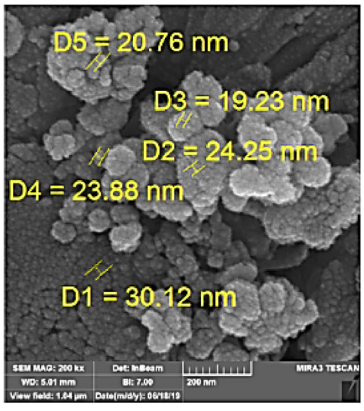
D5 = 20.76 nm
D3 = 19.23 nm
D2 = 24.25 nm
D4 = 23.88 nm
D1 = 30.12 nm

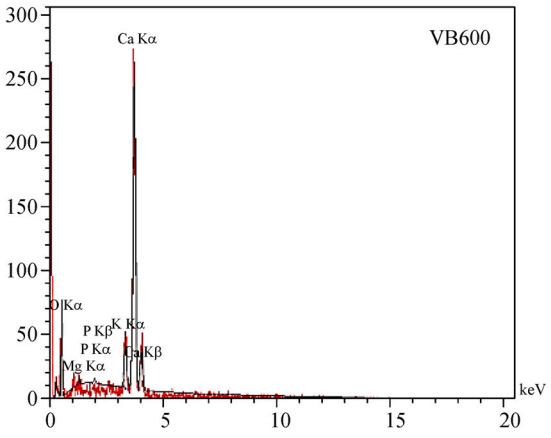
VB600
Ca Kα
O Kα
P Kβ
K Kα
P Kα
Ca Kβ
Mg Kα
keV

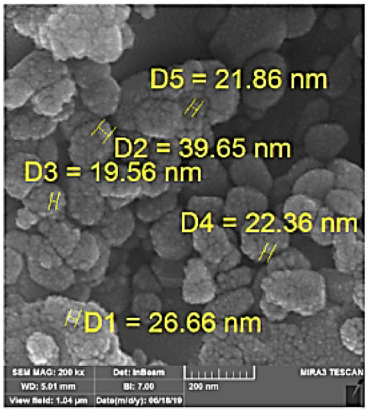
D5 = 21.86 nm
D2 = 39.65 nm
D3 = 19.56 nm
D4 = 22.36 nm
D1 = 26.66 nm

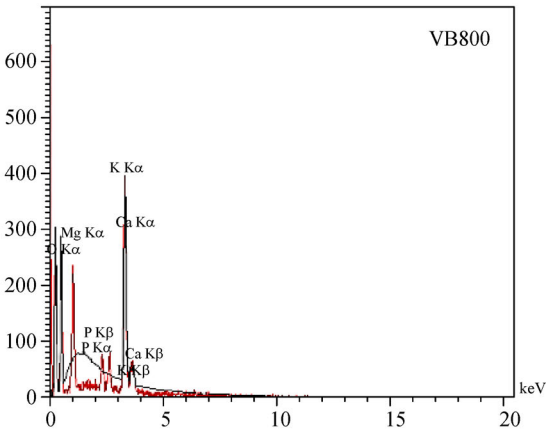
VB800
K Kα
Ca Kα
Mg Kα
O Kα
P Kβ
P Kα
Ca Kβ
K Kβ
keV

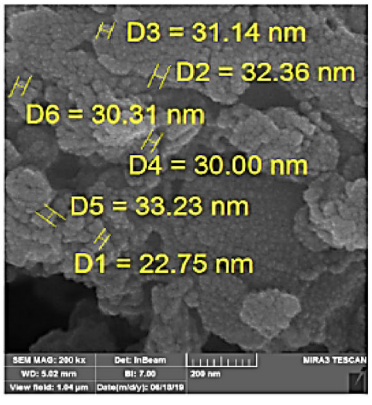
D3 = 31.14 nm
D2 = 32.36 nm
D6 = 30.31 nm
D4 = 30.00 nm
D5 = 33.23 nm
D1 = 22.75 nm

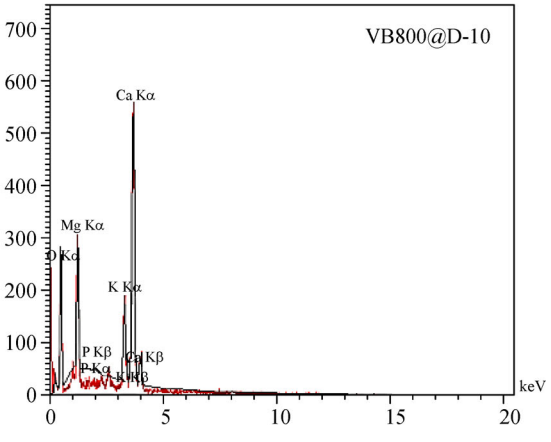
VB800@D-10
Ca Kα
Mg Kα
O Kα
K Kα
P Kβ
P Kα
Ca Kβ
K Kβ
keV

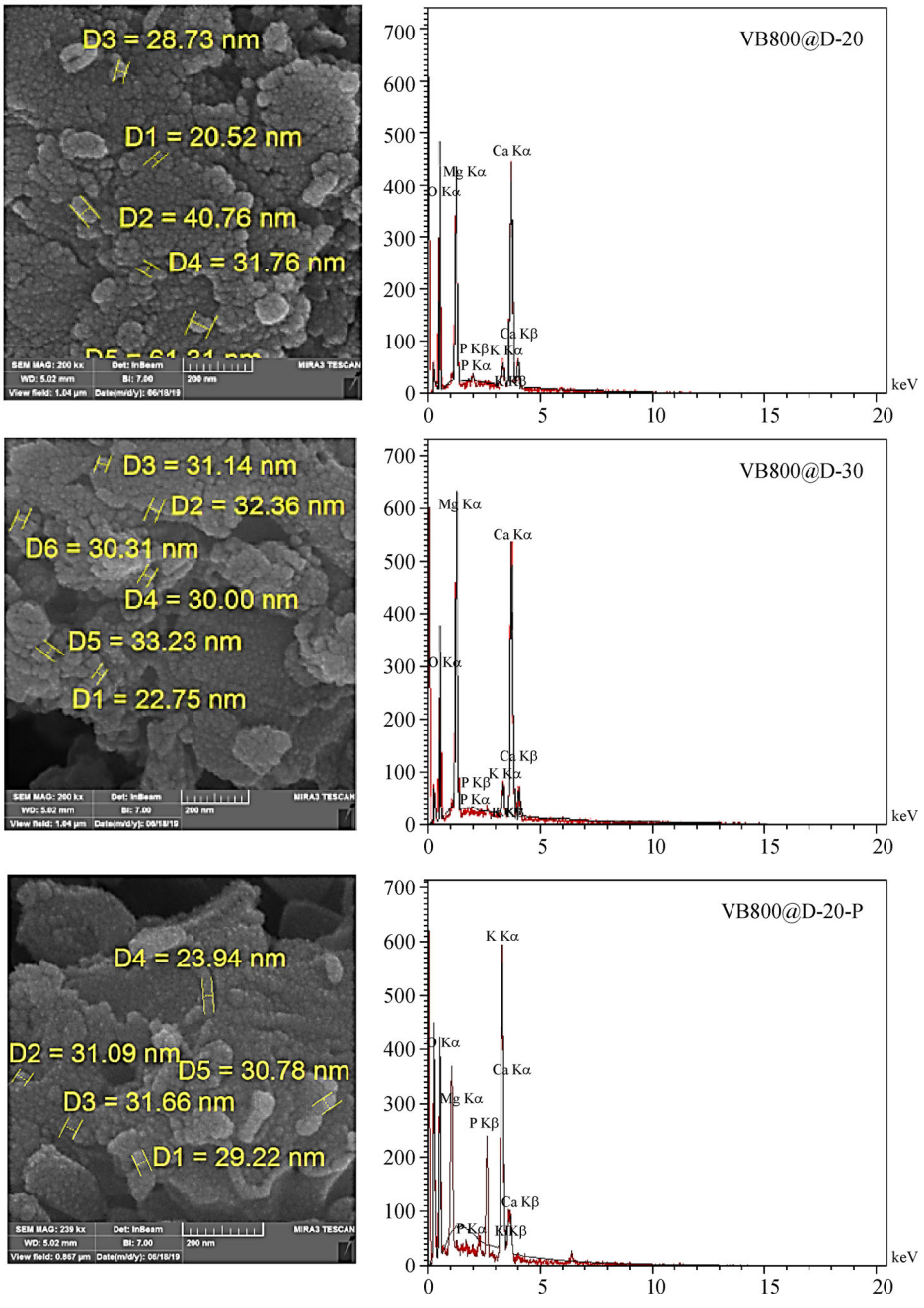

Fig. 2 SEM images and EDX spectra of prepared VB samples.

the surface and the formation of inner-sphere complexes with metal oxide on the surface.

Metal oxides have attracted extensive scientific interest for the remediation of anionic contamination (Manning and Goldberg, 1996). Metal oxide surfaces such as MgO and CaO become hydroxylated when they come into contact with water, inducing either a negative or positive charge depending on the pH of the solution. As known, phosphate acid () undergoes dissociation at different pHs, yielding different anionic species. The and forms of P prevail in the solution in the initial of the adsorption process, especially when the solution pH ranges between 3.00 and 9.00. Hence, the P anionic species could be removed from the solution owing to electrostatic interaction with protonated MOH^+ (M = Ca and Mg) on the surface of VB samples.

In aqueous media, most of the metal oxide was converted to metal hydroxide and complex compounds. As pH increased during the reaction, the affinity of the metal oxides on the VB surface to precipitate with P anions would be significantly enhanced, leading to $M(OH)_2$ precipitation and formation of M-P complexes.

Table 1 Elemental composition of the prepared VB samples

Adsorbents	SiO_2 (%)	Al_2O_3 (%)	Fe_2O_3 (%)	CaO (%)	Na_2O (%)	MgO (%)	K_2O (%)	TiO_2 (%)	MnO (%)	P_2O_5 (%)	LOI (%)	Cl (%)	SO_3 (%)
VB400	N	N	0.17	7.03	6.47	2.96	25.16	0.029	0.031	0.018	47.04	4.15	6.74
VB600	N	N	0.18	9.32	6.33	5.11	24.03	0.033	0.025	0.023	44.3	4.04	6.25
VB800	N	N	0.16	17.85	5.54	8.89	18.91	0.03	0.033	0.017	39.2	4	5
VB800@D-10	N	N	0.348	23.02	3.11	15.22	17.87	0.018	0.023	0.011	36.11	3	0.5
VB800@D-20	N	N	0.011	27.08	1.95	18.22	17.04	0.017	0.011	0.008	30.77	3.4	1.1
VB800@D-30	N	N	0.014	30.79	1.05	22.56	16.134	0.022	0.027	0.002	25.34	2.8	0.9
VB800@D-20/P	N	0.06	0.289	26.264	1.151	19.13	17.58	0.019	0.021	9.577	25.74	N	N

Table 2 Textural parameters of the prepared VB samples employed in this study

Adsorbents	S BET (m^2/g)	V total (cm^3/g)	Average pore size (nm)
VB400	61.3	0.07	1.1
VB600	84.69	0.15	1.25
VB800	128.21	0.32	1.65
VB800@D-10	119.11	0.28	1.45
VB800@D-20	107.45	0.25	1.32
VB800@D-30	85.27	0.22	1.16

It is also important to note that VB800 possesses a good adsorption capacity compared to VB600 and VB400 because of its higher specific surface area and small size and thus better capacity for P ions. Many studies have reported that the surface area and particle size of biochar-based adsorbents could make positive contributions to their performance (Takaya et al., 2016a). An increase of pyrolysis heat resulted in a significant increase in the specific surface area.

As can be seen in Fig. 3, the modified-VB800 exhibits a larger adsorption capacity than unmodified-VB800. Modification of VB800 with dolomite improved their adsorption capacities towards P ions.

The pre-treatment of dolomite, calcination at 1200 °C, had significant effects on P adsorption ability of dolomite (Salameh et al., 2015). The thermal decomposition behavior of dolomite was studied by a system including several of step reactions (Stefaniak et al., 2002). The disintegration of dolomite happens in two steps and could occur via either dissociation into magnesium carbonate ($MgCO_3$) and calcium carbonate ($CaCO_3$), followed by the disintegration of $MgCO_3$, or the dolomite skeleton degradation to the oxide combinations followed by re-formation of $CaCO_3$ by CaO re-carbonation.

The heating decomposition of dolomite is usually written as (Aparicio et al., 2017):

$$CaMg(CO_3)_2 = MgO + CaCO_3 + CO_2 \quad (19)$$

$$CaCO_3 = CaO + CO_2 \quad (20)$$

VB800@D-20 has a higher removal efficiency than VB800@D-10, because of increased active sites (metal oxides) causing in a high electrostatic interaction between the surface and P ions. As the dolomite further increased to 30 wt.%, a slight decline of BET surface area from 119.11 m^2/g to 85.27 m^2/g led to lowered P adsorption.

Among all the VB-samples produced in this work, the VB800@D-20 had the highest P adsorption which was then selected for further investigations.

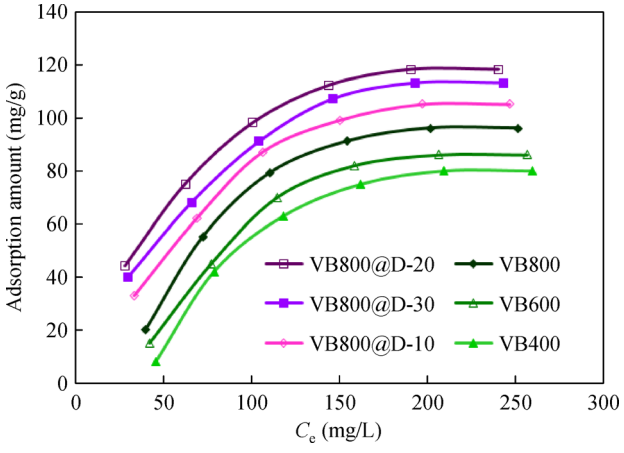

Fig. 3 Isotherm study for P ion adsorption on the prepared VB samples (reaction time = 90 min, applied VBs = 500 mg/L, pH = 7).

3.3 Optimization of adsorption conditions using RSM approach

The second-order polynomial response equation was suggested to correlate independent and dependent variables, which can be explained by the following equation:

$$q_e = +111.57 + 8.62A + 10.21B + 8.93C - 1.90AB - 0.095AC + 1.56BC - 51.43A^2 - 6.82B^2 - 11.42C^2 \quad (21)$$

where, q_e = equilibrium capacity of P adsorption (mg/g), A = pH, B = initial concentration of P (mg/L) and C = time

(min). The analysis of variance (ANOVA) for the P uptake has been summarized in Table S3 (in the supporting information file). An F-value (mean square for model/ mean square for the residual) of 454.40 with a low probability value ($p < 0.0001$) indicated a high significance for the regression model. There was only a 0.01% chance that the model F-value could occur because of noise. The signal to noise ratio was analyzed with adequate precision, with the proper range being >4. In this model, the adequate precision of 59.25 revealed a proportional signal which is often applied to navigate the design space.

The summary statistics shows that the pred R^2 of 0.9779 and adj R^2 of 0.9954 were in reasonable agreement with each other. Thus, all of these statistical models revealed that the developed quadratic model was proper for representing the data and able to provide an excellent description of the relationship between the response and process variables.

The effects of operating variables on the adsorption capacity of P from aqueous media by VB800@D-20 are illustrated by the 3D response surfaces in Fig. 4. The maximum P removal occurred when experimental conditions were set at 250 (mg/L) of P concentration, pH 7 and contact time 90 (min).

3.3.1 Effect of solution pH

To optimize the experimental conditions of P sorption onto VB800@D-20, the adsorption studies were done at five various initial pH levels. As known, P can exist in different ionic species, H_3PO_4, $H_2PO_4^-$, and PO_4^{3-}, depending on the solution pH with the pK_{a1}, pK_{a2}, and pK_{a3} for H_3PO_4 being 2.2, 7.2, and 12.4, respectively (Chen et al., 2016). The changes of P adsorption by VB800@D-20 against pH are shown in Fig. 4. The P removal of the prepared nanocomposite increased as pH rose within 3.00–6.00, reaching the maximum adsorption within the pH range 6.00–9.00 and then declining as pH increased from 9.00 to 11.00. P species exist in neutral form (H_3PO_4) at pH 2, thus the lower uptake ability may be because of the lack of electrostatic forces. At pH between 5 and 7, the P is excited as anionic species ($H_2PO_4^-$ and HPO_4^{2-}) while due to the protonation, the adsorbent surface was positively charged. Thus, the anionic P species were attached to the VB800@D-20 via electrostatic attraction between P anions and the positive charges on the surface. At pH > 9.0, the reduction in uptake was because of the competition of OH^- ions with the P species (PO_4^{3-}).

3.3.2 Effect of initial concentration and adsorption isotherm

As observed in Fig. 4(a), upon elevation of the P concentration at the beginning of the tests, its adsorption onto VB800@D-20 nanocomposite was enhanced, and the equilibrium curves displayed a slow ascending trend when the concentration of P ion was about 250 mg/L. This further suggests that the mass transfer force of P ions between the solution and VB800@D-20 improved with the increase in the initial concentration. The adsorption isotherm of VB800@D-20 was measured to evaluate its P adsorption performance based on P concentration with the fitting conditions and parameters for D-R, Freundlich, Langmuir, and models listed Table S4.

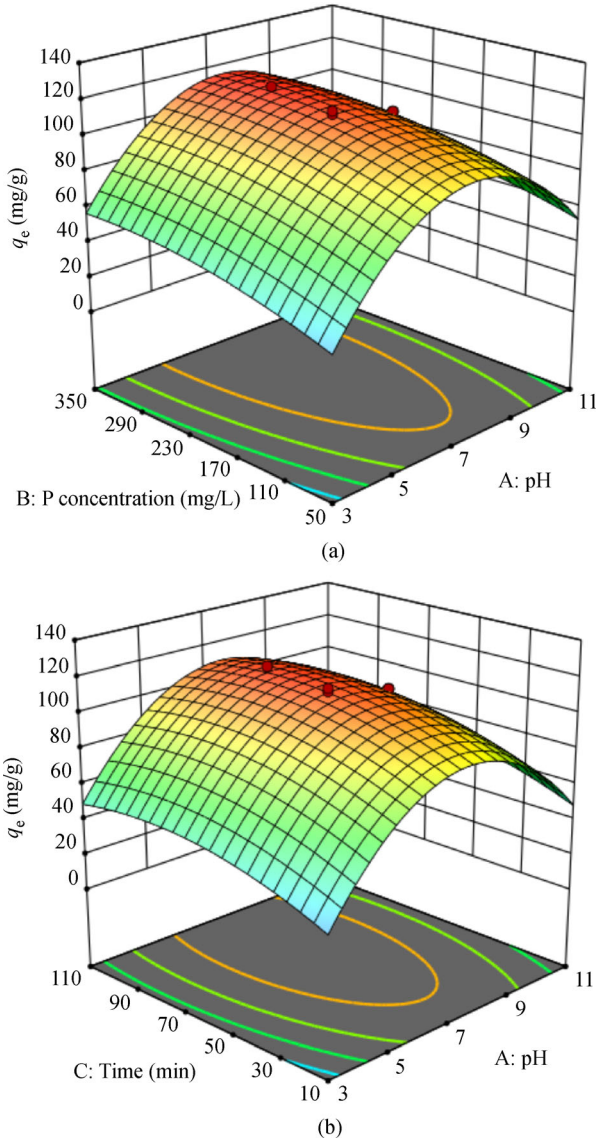

Fig. 4 Combined effects of (a) P concentration and pH and (b) reaction time and pH on the equilibrium capacity of adsorption.

According to the data listed in Table S4, it is also seen that the Langmuir isotherm could model the experimental data better than the others with the highest correlation coefficients (R^2). Thus, the adsorption is more likely to occur on a monolayer surface, and there is no considerable interaction between the adsorbed components. Further, the R_L value of Langmuir for studied P anions has fallen

within the range of 0–1, indicating that the adsorption process was favorable. This result is also confirmed by the "n" parameter of the Freundlich model being within the range of 1–10. The Freundlich exponent n value was estimated to 1.72. The E values from D-R isotherm model have been larger than 8 kJ/mol (~10.66 kJ/mol), demonstrating the chemisorption of the process.

Since the q_m is a significant variable to optimize the process of adsorbing pollutants, a comparison was made in Table 3 between q_m of VB800@D-20 in P ion removal with the other adsorbents of previous studies. According to this table, VB800@D-20 could be considered as an attractive and promising material for nutrients and in particular P recovery from aqueous media.

3.3.3 Effect of contact time and adsorption kinetics

The amount of adsorbed P increased rapidly in the initial stage of the P adsorption reaction, probably due to the presence of huge vacant active sites on the VB800@D-20 nanocomposite surface (Fig. 4(b)). However, the adsorption rate became slower in response to diminished vacant active sites with adsorption time.

To investigate the kinetics of adsorption of P ions on VB800@D-20, five models have been considered, i.e. pseudo-first-order, pseudo-second-order, Elovich, intraparticle diffusion and particle diffusion models.

The different parameters as well as the corresponding R^2 of five kinetic models are listed in Table 4. Based on the data reported in Table 4, it is also observed that the P adsorption on VB800@D-20 was better described by the pseudo-second-order kinetic model with the greatest R^2 among the five models. The adsorption mechanism best matched the pseudo-second-order model suggesting that the process is mainly controlled by chemisorption. This indicates that P adsorption onto the VB800@D-20 involves valency forces via exchanging or sharing electrons between VB800@D-20 and P ions.

3.4 Effect of temperature and thermodynamic study

The P ions removal by VB800@D-20 nanocomposite was affected by the experimental temperature with these variations displayed in Table 4. According to this table, with the increase in the temperature from 298 K to 348 K, the amount of P adsorbed onto the prepared nanocomposite decreased from 118 to 99 mg/g. The reduced removal of P ions during this process could be attributed to the accelerated desorption from the surface occurring at higher temperatures causing the increased tendency of the P species to escape from the VB800@D-20 surface to the solution phase; thus, the amount of P ions adsorbed declined.

The thermodynamic parameters and the correlation coefficients (R^2) are presented in Table 4. ΔGs were negative at three temperature stages revealing the spontaneous and favorable nature of P adsorption onto VB800@D-20. Further, ΔG dropped from about −20 to −23 kJ/mol due to temperature increment from 298 K to 348 K, representing the augmented spontaneity at higher temperatures. The ΔH became negative indicating the P adsorption onto VB800@D-20 has an exothermic nature. The ΔS value was positive implying increased randomness during the ongoing process and accordingly a good affinity

Table 3 P uptakes onto various adsorbents.

Adsorbents	q_m (mg/g)	References
Mg-enriched tomato tissues	116.60	Yao et al. (2013)
Ca–Mg loaded biochar	326.62	Fang et al. (2015)
MgO-impregnated magnetic biochar	121.25	Li et al. (2016b)
CaO-MgO Carbon hybrid composite	207.79	Li et al. (2018a)
Mg/Al-LDHs biochar	81.83	Li et al. 2016a)
biochar calcium-alginate beads	214.20	Jung et al. (2017)
La_2O_3 grafted oak biochar	142.70	Wang et al. (2015)
Laminaria japonica-derived biochar	132.39	Jung et al. (2016)
Laminaria japonica-derived biochar (LB)-calcium alginate beads	126.71	Jung et al. (2016)
Magnesium hydroxide modified Diatomite	45.70	Mitrogiannis et al. (2017)
Calcium-rich biochar	147.05	Antunes et al. (2018)
Calcium decorated sludge carbon	116.82	Kong et al. (2018)
Mg oak biochar (in situ)	64.60	Takaya et al. (2016b)
Mg GHW biochar (in situ)	65.10	Takaya et al. (2016b)
Fe–Mn binary oxide	36.00	Rodrigues and da Silva (2010)
VB800@D-20	178.57	This study

Table 4 Adsorption kinetic and thermodynamic parameters for P adsorption on VB800@D-20.

Model	Parameter	Unit		Value	
Pseudo-first-order	K_1	L/min		0.0376	
	q_e	mg/g		136.03	
	R^2			0.9821	
Pseudo-second-order	K_2	g/mg/min		0.00015	
	q_e	mg/g		166.66	
	R^2			0.9994	
Elovich	β			0.0254	
	α			1.146	
	R^2			0.9987	
Intra-particle diffusion	K_{int}	g/mg/min$^{0.5}$		0.0751	
	R^2			0.9923	
Particle diffusion	K_p	min^{-1}		0.0376	
	R^2			0.9821	
Thermodynamic parameters	T	K	298	323	348
	q_e	mg/g	118	106	99
	ΔG	kJ/mol	–20.03	–21.39	–22.75
	ΔH	kJ/mol		–3.86	
	ΔS	kJ/mol/K		0.0542	
	R^2			0.9992	

of P with the adsorbent. A similar result has been reported for P uptake on Mg-Al hydrotalcite-loaded kaolin (Deng and Shi, 2015).

3.5 Co-existing anions

The influence of commonly present anions such as nitrate (NO_3^-), chloride (Cl^-), sulfate (SO_4^{2-}), and carbonate (CO_3^{2-}) on P removal by VB800@D-20 was studied with the corresponding result demonstrated in Fig. S1. Specifically, 0.01 g of VB800@D-20 at pH 7 was added to a 20 mL of solution with 250 mg/L of P and 250 mg/L of the specific anion on each co-existing anion experiment and stirred for 90 min. Based on Fig. S1, the P uptake decreased slightly with co-presence of Cl^- and NO_3^- while it dropped significantly in the co-presence of CO_3^{2-} and SO_4^{2-}. Note that some anions would compete with P to grab the active vacancies and some would increase the repulsive forces. Indeed, multivalent anions are adsorbed more easily than monovalent anions. The favorable performance of the VB800@D-20 nanocomposite on the tolerance of co-existing anions suggested that the prepared nanocomposite possessed highly selective adsorption towards P, thus offering a great potential in wastewater treatment.

3.6 Desorption and reusability

Desorption studies were conducted using P-adsorbed VB800@D-20 at different HCl concentrations (0.1–2.0 M). It was found that ~79.0%, ~87.0%, ~94.0%, and ~94.0% P oxyanions were released in 0.1 M HCl, 0.5 M HCl, 1.0 M HCl, and 2.0 M HCl solutions, respectively. Based on obtained results, the amount of the desorbed P increased with raising the HCl concentration. Further enhancement of HCl concentration to 2.0 M, however, did not show obvious increase in the P release. According to these observations, 1.0 M was selected as a suitable value for the desorption of P ions in this study. The regenerated VB800@D-20 was washed with deionized water five times before the next cycle of adsorption and desorption. This procedure was repeated for five cycles determining spent adsorbent reclaimability and the corresponding results are presented in Fig. S2. In the previous three cycles, the adsorbed P could be extracted by the 1.0 M HCl solution and there was a negligible change in the adsorption capacity of VB800@D-20. After five subsequent recycles, the amount of adsorbed P on VB800@D-20 slightly decreased to ~84% of the original value, implying that part of the active sites was lost. The results obtained indicate that, after the recovery of adsorbed P ions, the regenerated

VB800@D-20 nanocomposite could be reused for the efficient P recovery from the aqueous solution.

3.7 Nanocomposite biochar P-loaded reuse as a P-fertilizer

As described in section 2.6, the potential of P- loaded biochar to be used as a substitute to P-fertilizer was assessed by the release rate and assessment of its effect on the plant growth. As adsorption was a pH-sensitive process, desorption of phosphate is also a function of pH. The release rate in DI water at different pH has been as illustrated in Fig. 5(a). As the adsorption showed better efficiency on neutral and alkaline conditions, it was not surprising that desorption would occur in an acidic solution. It was mentioned in previous studies that the recovered phosphorus in the presence of Mg and Ca, is released in acidic condition or adsorbed P on biochar is a proper fertilizer in acidic soil (Fang et al., 2015; Kataki et al., 2016).

Another assessment for better understanding the effect of using the P-loaded nanocomposite biochar as a substitution for phosphorus fertilizer was a pot experiment, described previously, comparing its effect on the plant growth. As shown in Fig. 5(b), P-loaded biochar could effectively play an important role in plant height and biomass weight. It increased the dry weight of biomass by 67% and the above soil height by 49% (Table S5).

This study indicated that vinasse-dolomite nanocomposite biochar was first able to remove phosphate, and could also be used as a phosphorus fertilizer alternative and deliver its adsorbed phosphate as a bio-available element during plant growth.

4 Conclusions

In the present work, biochars were produced from vinasse through pyrolysis at different temperatures. With the rise of the pyrolysis temperature from 400°C to 800°C, the VB samples revealed a gradual rise in the amount of P removal. The VB-dolomite nanocomposites were fabricated by a facile method and employed as a highly suitable adsorbent

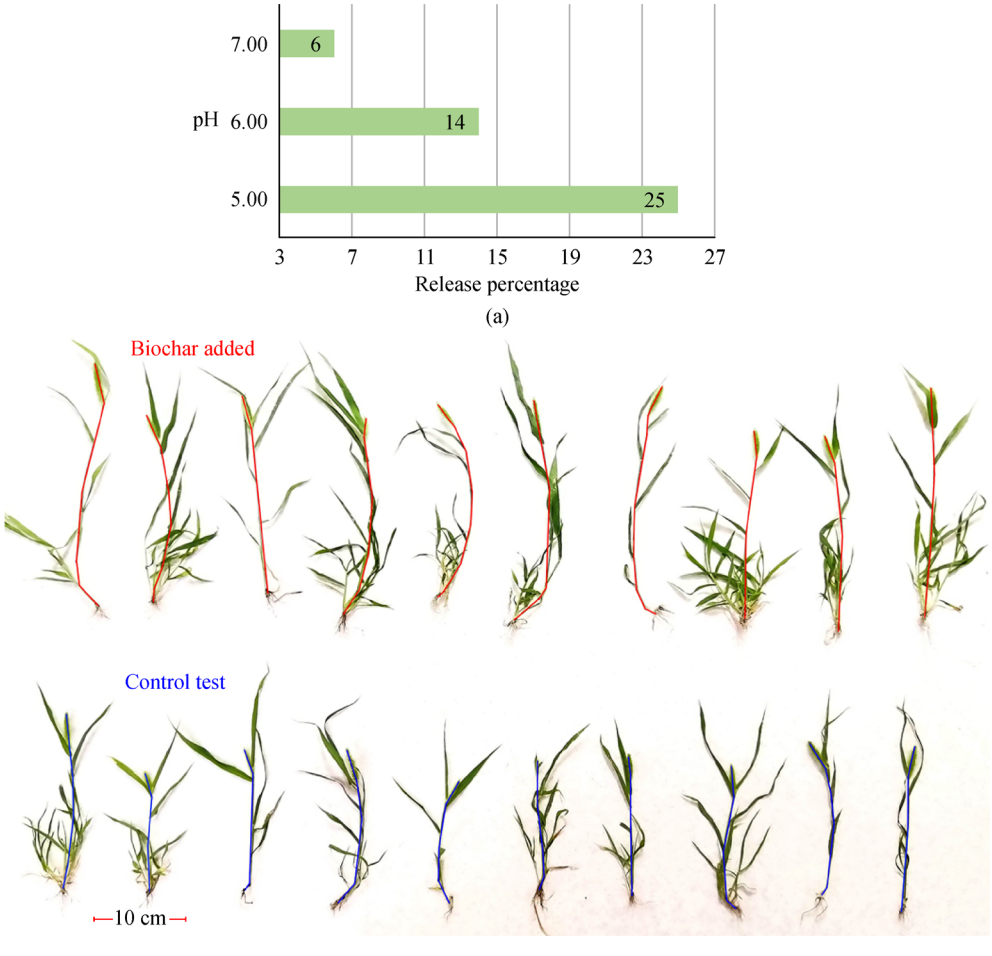

Fig. 5 VB800@D-20/P release test in DI (a) and effect on *Setaria viridis* (b).

for adsorbing P. The structure, morphology, and surface properties of the synthesized VB samples were characterized by XRD, FT-IR, XRF, SEM-EDX and N_2 adsorption/desorption. VB800@D-20 showed higher adsorption capacity toward P ion compared to the other prepared adsorbents in the adsorption experiment data. The experimental design was performed using the RSM based on CCD reducing the repetition of experiments, and to obtain the optimum values for VB800@D-20 as the selected adsorbent. The optimal operational parameters were obtained as 250 (mg/L) of P concentration with 90 min as reaction time at pH 7. The adsorption capacity of VB800@D-20 toward P ion diminished with temperature rise from 298 K to 348 K. The thermodynamic study data indicated that the removal process has an exothermic and spontaneous nature. The data from isotherm study well matched the Langmuir model than the D-R or the Freundlich models, suggesting that the adsorption may be monolayer. A q_{max} of 178.57 mg/g at 298 K was achieved according to the Langmuir model. Application of different adsorption kinetic models to obtain the adsorption kinetics of P onto VB800@D-20 revealed that the second-order model could explain the experimental data better than others. The overall adsorption tendency of the synthesized VB800@D-20 nanocomposite toward P in the presence of NO_3^-, Cl^-, SO_4^{2-} and CO_3^{2-} under competitive conditions, followed the order: $NO_3^- > Cl^- > SO_4^{2-} > CO_3^{2-}$. Desorption experiments proved that the P species are more readily released when being subject to HCl 1.0 M. The P adsorption capacity after five adsorption–desorption cycles demonstrated the high potential of VB800@D-20 for P adsorption in fifth cycles without notable adsorption capacity reduction in comparison with the first cycle. The VB800@D-20 nanocomposite is an efficient adsorbent for P ion removal, further being potential of a P fertilizer.

Electronic Supplementary Material Supplementary material is available in the online version of this article at https://doi.org/10.1007/s11783-020-1249-6 and is accessible for authorized users.

References

Aksu Z, Gönen F (2006). Binary biosorption of phenol and chromium (VI) onto immobilized activated sludge in a packed bed: Prediction of kinetic parameters and breakthrough curves. Separation and Purification Technology, 49(3): 205–216

Anbia M, Rahimi F (2017). Adsorption of platinum(IV) from an aqueous solution with magnetic cellulose functionalized with thiol and amine as a nano-active adsorbent. Journal of Applied Polymer Science, 134(39): 45361

Antunes E, Jacob M V, Brodie G, Schneider P A (2018). Isotherms, kinetics and mechanism analysis of phosphorus recovery from aqueous solution by calcium-rich biochar produced from biosolids via microwave pyrolysis. Journal of Environmental Chemical Engineering, 6(1): 395–403

Aparicio J D, Benimeli C S, Almeida C A, Polti M A, Colin V L (2017). Integral use of sugarcane vinasse for biomass production of actinobacteria: Potential application in soil remediation. Chemosphere, 181: 478–484

Boeykens S, Piol M, Legal L, Saralegui A B, Vázquez C (2017). Eutrophication decrease: Phosphate adsorption processes in presence of nitrates. Journal of Environmental Management, 203

Chen M, Huo C, Li Y, Wang J (2016). Selective adsorption and efficient removal of phosphate from aqueous medium with graphene–lanthanum composite. ACS Sustainable Chemistry & Engineering, 4(3): 1296–1302

Chen T, Zhang Y, Wang H, Lu W, Zhou Z, Zhang Y, Ren L (2014). Influence of pyrolysis temperature on characteristics and heavy metal adsorptive performance of biochar derived from municipal sewage sludge. Bioresource Technology, 164: 47–54

Chowdhary P, Yadav A, Kaithwas G, Bharagava R N (2017). Green Technologies and Environmental Sustainability. Singh R and Kumar S, eds. Cham: Springer International Publishing,409–435

Christofoletti C, Pedro Escher J, Correia J, Fernanda Urbano Marinho J, Silvia Fontanetti C (2013). Sugarcane vinasse: Environmental implications of its use. Waste Management, 33(12): 2752–2761

Creech J E, Monaco T A, Evans J O (2004). Photosynthetic and growth responses of zea mays L and four weed species following post-emergence treatments with mesotrione and atrazinet. Pest Manag Sci, 60(11): 1079–1084

Deng L, Shi Z (2015). Synthesis and characterization of a novel Mg–Al hydrotalcite-loaded kaolin clay and its adsorption properties for phosphate in aqueous solution. Journal of Alloys and Compounds, 637: 188–196

Dubinin M,Radushkevich L V (1947). The equation of the characteristic curve of activated charcoal. Proceedings of the Union of Soviet Socialist Republics Academy of Sciences, 55: 331–337

Fang C, Zhang T, Li P, Jiang R, Wu S, Nie H, Wang Y (2015). Phosphorus recovery from biogas fermentation liquid by Ca–Mg loaded biochar. Journal of Environmental Sciences (China), 29: 106–114

Freundlich H (1907). Über die adsorption in lösungen. Zeitschrift für Physikalische Chemie, 57(1): 385–470

Fukushima N A, Palacios-Bereche M C, Palacios-Bereche R, Nebra S A (2019). Energy analysis of the ethanol industry considering vinasse concentration and incineration. Renewable Energy, 142: 96–109

Hoarau J, Caro Y, Grondin I, Petit T (2018). Sugarcane vinasse processing: Toward a status shift from waste to valuable resource. A review. Journal of Water Process Engineering, 24: 11–25

Huang H, Liu J, Zhang P, Zhang D, Gao F (2017a). Investigation on the simultaneous removal of fluoride, ammonia nitrogen and phosphate from semiconductor wastewater using chemical precipitation. Chemical Engineering Journal, 307: 696–706

Huang W, Zhang Y, Li D (2017b). Adsorptive removal of phosphate from water using mesoporous materials: A review. Journal of Environmental Management, 193: 470–482

Jung K W, Jeong T U, Choi J W, Ahn K H, Lee S H (2017). Adsorption of phosphate from aqueous solution using electrochemically modified biochar calcium-alginate beads: Batch and fixed-bed column performance. Bioresource Technology, 244: 23–32

Jung K W, Jeong T U, Kang H J, Ahn K H (2016). Characteristics of biochar derived from marine macroalgae and fabrication of granular biochar by entrapment in calcium-alginate beads for phosphate removal from aqueous solution. Bioresource Technology, 211: 108–116

Karimifard S, Alavi Moghaddam M R (2018). Application of response surface methodology in physicochemical removal of dyes from wastewater: A critical review. Science of the Total Environment, 640–641: 772–797

Kataki S, West H, Clarke M, Baruah D C (2016). Phosphorus recovery as struvite: Recent concerns for use of seed, alternative Mg source, nitrogen conservation and fertilizer potential. Resources, Conservation and Recycling, 107: 142–156

Kazak O, Ramazan Eker Y, Bingol H, Tor A (2017). Preparation of activated carbon from molasses-to-ethanol process waste vinasse and its performance as adsorbent material. Bioresource Technology, 241: 1077–1083

Kong L, Han M, Shih K, Su M, Diao Z, Long J, Chen D, Hou L A, Peng Y (2018). Nano-rod Ca-decorated sludge derived carbon for removal of phosphorus. Environmental Pollution, 233: 698–705

Langmuir I (1918). The adsorption of gases on plane surfaces of glass, mica and platinum. Journal of the American Chemical Society, 40(9): 1361–1403

Li R, Wang J J, Zhang Z, Awasthi M K, Du D, Dang P, Huang Q, Zhang Y, Wang L (2018a). Recovery of phosphate and dissolved organic matter from aqueous solution using a novel CaO-MgO hybrid carbon composite and its feasibility in phosphorus recycling. Science of the Total Environment, 642: 526–536

Li R, Wang J J, Zhou B, Awasthi M K, Ali A, Zhang Z, Gaston L A, Lahori A H, Mahar A (2016a). Enhancing phosphate adsorption by Mg/Al layered double hydroxide functionalized biochar with different Mg/Al ratios. Science of the Total Environment, 559: 121–129

Li R, Wang J J, Zhou B, Awasthi M K, Ali A, Zhang Z, Lahori A H, Mahar A (2016b). Recovery of phosphate from aqueous solution by magnesium oxide decorated magnetic biochar and its potential as phosphate-based fertilizer substitute. Bioresource Technology, 215: 209–214

Li Z, Qiu Z, Yang J, Ma B, Lu S, Qin C (2018b). Investigation of phosphate adsorption from an aqueous solution using spent fluid catalytic cracking catalyst containing lanthanum. Frontiers of Environmental Science & Engineering, 12(6): 15

López R, Antelo J, Fiol S, Macías-García F (2019). Phosphate adsorption on an industrial residue and subsequent use as an amendment for phosphorous deficient soils. Journal of Cleaner Production, 230: 844–853

Manning B A, Goldberg S (1996). Modeling competitive adsorption of arsenate with phosphate and molybdate on oxide minerals. Soil Science Society of America Journal, 60(1): 121–131

Mitrogiannis D, Psychoyou M, Baziotis I, Inglezakis V J, Koukouzas N, Tsoukalas N, Palles D, Kamitsos E, Oikonomou G, Markou G (2017). Removal of phosphate from aqueous solutions by adsorption onto $Ca(OH)_2$ treated natural clinoptilolite. Chemical Engineering Journal, 320: 510–522

Nugroho F L, Mulyatna L, Situmeang A D W (2014). Removal of phosphate from synthetic aqueous solution by adsorption with dolomite from Padalarang. Journal of Engineering and Technological Sciences, 46(4): 410–419

Pradel M, Aissani L (2019). Environmental impacts of phosphorus recovery from a "product" Life Cycle Assessment perspective: Allocating burdens of wastewater treatment in the production of sludge-based phosphate fertilizers. Science of the Total Environment, 656: 55–69

Ren S, Li M, Sun J, Bian Y, Zuo K, Zhang X, Liang P, Huang X (2017). A novel electrochemical reactor for nitrogen and phosphorus recovery from domestic wastewater. Frontiers of Environmental Science & Engineering, 11(4): 17

Rodrigues L A, Da Silva M L C P (2010). Thermodynamic and kinetic investigations of phosphate adsorption onto hydrous niobium oxide prepared by homogeneous solution method. Desalination, 263(1): 29–35

Salameh Y, Albadarin A B, Allen S, Walker G, Ahmad M (2015). Arsenic (III, V) adsorption onto charred dolomite: Charring optimization and batch studies. Chemical Engineering Journal, 259: 663–671

Selim A Q, Sellaoui L, Mobarak M (2019). Statistical physics modeling of phosphate adsorption onto chemically modified carbonaceous clay. Journal of Molecular Liquids, 279: 94–107

Shahid M K, Kim Y, Choi Y G (2019). Adsorption of phosphate on magnetite-enriched particles (MEP) separated from the mill scale. Frontiers of Environmental Science & Engineering, 13(5): 71

Sivakumar P, Palanisamy P (2009). Adsorption studies of basic Red 29 by a non-conventional activated carbon prepared from *Euphorbia antiquorum* L. International Journal of Chemtech Research, 1(3): 502–510

Stefaniak E, Biliński B, Dobrowolski R, Staszczuk P, Wojcik J (2002). The influence of preparation conditions on adsorption properties and porosity of dolomite-based sorbents. Colloids and Surfaces. A, Physicochemical and Engineering Aspects, 208(1–3): 337–345

Sun G, Zhang C, Li W, Yuan L, He S, Wang L (2018). Effect of chemical dose on phosphorus removal and membrane fouling control in a UCT-MBR. Frontiers of Environmental Science & Engineering, 13(1): 1

Takaya C, Fletcher L, Singh S, Anyikude K, Ross A (2016a). Phosphate and ammonium sorption capacity of biochar and hydrochar from different wastes. Chemosphere, 145: 518–527

Takaya C, Fletcher L, Singh S, Okwuosa U, Ross A (2016b). Recovery of phosphate with chemically modified biochars. Journal of Environmental Chemical Engineering, 4(1): 1156–1165

Tripathi M, Sahu J N, Ganesan P (2016). Effect of process parameters on production of biochar from biomass waste through pyrolysis: A review. Renewable & Sustainable Energy Reviews, 55: 467–481

Valle L R, Rodrigues S L, Ramos S J, Pereira H S, Amaral D C, Siqueira J O, Guilherme L R G (2016). Beneficial use of a by-product from the phosphate fertilizer industry in tropical soils: Effects on soil properties and maize and soybean growth. Journal of Cleaner Production, 112: 113–120

Vikrant K, Kim K H, Ok Y S, Tsang D C W, Tsang Y F, Giri B S, Singh R S (2018). Engineered/designer biochar for the removal of phosphate in water and wastewater. Science of the Total Environment, 616–617: 1242–1260

Wang J, Wang S (2019). Preparation, modification and environmental application of biochar: A review. Journal of Cleaner Production, 227: 1002–1022

Wang Z, Guo H, Shen F, Yang G, Zhang Y, Zeng Y, Wang L, Xiao H, Deng S (2015). Biochar produced from oak sawdust by Lanthanum (La)-involved pyrolysis for adsorption of ammonium (NH_4^+), nitrate (NO_3^-), and phosphate (PO_4^{3-}). Chemosphere, 119: 646–653

Xue Y, Wang C, Hu Z, Zhou Y, Xiao Y, Wang T (2019). Pyrolysis of sewage sludge by electromagnetic induction: Biochar properties and application in adsorption removal of Pb(II), Cd(II) from aqueous solution. Waste Management (New York, N.Y.), 89: 48–56

Yao Y, Gao B, Chen J, Yang L (2013). Engineered biochar reclaiming phosphate from aqueous solutions: Mechanisms and potential application as a slow-release fertilizer. Environmental Science & Technology, 47(15): 8700–8708

Ye Y, Ngo H H, Guo W, Liu Y, Zhang X, Guo J, Ni B J, Chang S W, Nguyen D D (2016). Insight into biological phosphate recovery from sewage. Bioresource Technology, 218: 874–881

Zhao W, Shen A, Qiao Z, Pan L, Hu A, Zhang J (2018). Genetic types and distinguished characteristics of dolomite and the origin of dolomite reservoirs. Petroleum Exploration and Development, 45(6): 983–997